Mechanical Performance and Fracture Morphology of Fused Deposition Modeling-Printed Porous PLA Gyroid Architectures

Shaiful Anwar bin Ismail[1*], Wan Nur Aziah Najihah Binti Wan Mohamed Farikh[1], Mohd Fa'iz Bin Wahid[1], M.B. Ali[1], Mohd Hadzley Abu Bakar[1], Azrina Arshad[2], Piyanut Muangtong[3]

[1]Faculty of Industrial and Manufacturing Technology and Engineering, Universiti Teknikal Malaysia Melaka, Hang Tuah Jaya, 76100 Durian Tunggal, Melaka, Malaysia

[2]Oil and Gas section, Malaysian Institute of Industrial Technology, Universiti Kuala Lumpur, 81750 Johor Bahru, Johor, Malaysia

[3]Department of Materials Engineering, Faculty of Engineering, Rajamangala University of Technology Rattanakosin, 96 Phutthamonthon Sai 5 Rd., Salaya, Phutthamonthon, Nakhon Pathom, 73170, Thailand

***Corresponding Author**

DOI: https://doi.org/10.47772/IJRISS.2026.100701129

Received: 06 August 2026; Accepted: 11 August 2026; Published: 22 August 2026

ABSTRACT

Porous polymeric architecture fabricated via Fused Deposition Modeling (FDM) offers significant potential for lightweight engineering components and biomedical scaffolds due to their controllable internal topologies. Triply periodic minimal surface (TPMS) gyroid structures have emerged as a promising design strategy for lightweight components and biomedical scaffolds due to their continuous porous architecture, high surface-to-volume ratio, and efficient load distribution characteristics. However, the combined influence of Fused Deposition Modeling (FDM) process parameters on the mechanical behavior and failure mechanisms of gyroid-based structures remains insufficiently understood. Therefore, this study investigates the effects of infill density (30%, 50%, and 70%) and layer thickness (0.3, 0.4, and 0.5 mm) on the mechanical performance of polylactic acid (PLA) specimens incorporating a TPMS gyroid infill architecture. Specimens were fabricated using a CreatBot D1000 industrial FDM printer and evaluated through tensile and flexural testing according to ASTM D638 and ASTM D790 standards, respectively, with fully solid (100% infill) specimens serving as controls. Fracture morphology and pore characteristics were further analysed using Field Emission Scanning Electron Microscopy (FESEM). The results showed that both infill density and layer thickness significantly affected the structural performance of the gyroid specimens. The configuration with 70% infill density and 0.5 mm layer thickness achieved the highest tensile strength (33.24 MPa) and flexural strength (66.87 MPa), retaining approximately 70.4% of the strength of fully solid specimens while reducing material consumption by 30%. FESEM observations revealed predominantly cohesive trans-filament fracture in high-density gyroid structures, indicating improved inter-bead bonding, whereas low-density specimens (30% infill) exhibited stress concentration, interlayer delamination, and filament pull-out. The continuous gyroid architecture promoted uniform stress distribution and enhanced mechanical efficiency, demonstrating its suitability for lightweight load-bearing applications. These findings provide practical guidelines for optimizing FDM processing parameters in the fabrication of high-performance TPMS gyroid structures

Keyword: Triply Periodic Minimal Surface (TPMS); Gyroid Structure; Polylactic Acid (PLA); Infill Density; Mechanical Characterization.

INTRODUCTION

Porous architecture has attracted considerable interest in aerospace, automotive, energy absorption, and biomedical engineering because their structural performance can be tailored through controlled geometry, relative density, and material distribution. In tissue engineering, interconnected porous networks are particularly important because they promote nutrient diffusion, cellular infiltration, extracellular-matrix formation, and vascularization(Pan & Ding, 2012). Nevertheless, increasing porosity generally improves mass transport and permeability at the expense of stiffness, strength, and structural stability. This inherent trade-off makes the rational design of porous scaffolds a critical challenge, especially when the scaffold must provide both biological functionality and sufficient mechanical integrity during tissue regeneration. Consequently, the design of porous structures requires an appropriate balance between permeability, biological functionality, weight reduction, and mechanical integrity.

Among biodegradable polymers, Poly(lactic acid) (PLA) is one of the most widely used biodegradable thermoplastics for additive manufacturing because it is derived from renewable resources (Calabrese et al., 2025), exhibits comparatively low processing temperatures, and possesses a favorable combination of stiffness, dimensional stability, and biocompatibility (de Mulder et al., 2009). These characteristics have supported its application in biomedical prototypes, tissue-engineering scaffolds, and lightweight structural components. The mechanical properties of PLA parts produced by FFF/FDM are strongly dependent on the thermal and processing conditions experienced during fabrication. Parameters such as build direction, build orientation, layer thickness, and specimen thickness significantly influence interlayer adhesion and structural performance (Marşavina et al., 2022). Insufficient molecular diffusion between adjacent layers, incomplete fusion, residual porosity, and inconsistencies in bead geometry may result in pronounced anisotropic behavior and reduced mechanical strength, ultimately promoting premature failure (de Mulder et al., 2009).

FDM offers a cost-effective and accessible approach for fabricating customized porous structures directly from computer-aided design models, without the need for dedicated molds or extensive tooling. Compared with traditional manufacturing techniques, FDM-produced parts typically exhibit reduced mechanical performance owing to layer discontinuities, internal voids, and poor interlayer bonding. Print process parameters play a critical role in determining this performance, as they directly affect the structural integrity, density, and adhesion between successive layers (Cojocaru et al., 2022; Ekşi & Karakaya, 2025; Megersa et al., 2024). The process also enables the fabrication of complex internal architectures that are difficult to manufacture using conventional subtractive or molding techniques.

The final performance of an FDM-printed PLA samples structure is governed by the interaction between material properties, architectural design, and process parameters. Layer thickness, infill or relative density, raster configuration, nozzle temperature, extrusion rate, printing speed, and build orientation can influence interlayer bonding, dimensional accuracy, internal porosity, surface morphology, and mechanical anisotropy. However, the mechanical performance of PLA can be limited, particularly under high-stress conditions (Calabrese et al., 2025). Studies (Tang et al., 2020)have shown that layer thickness and infill-related parameters can substantially alter the tensile and bending performance of PLA parts, while changes in nozzle temperature and extrusion conditions influence the quality of interfacial bonding and the formation of defects. Fracture surface observations demonstrated that samples exhibiting homogeneous filament fusion and reduced porosity achieved superior mechanical performance. In contrast, specimens with weak interfacial bonding, characterized by delamination and interfacial separation, showed diminished strength and earlier failure (Ötüken et al., 2026).

The architecture of a porous structure is a critical factor governing its mechanical performance and deformation behaviour. Conventional porous patterns, such as grid, line, and cross configurations, often contain sharp intersections and abrupt changes in load-transfer direction, which can induce localized stress concentrations and non-uniform deformation under loading. As an alternative, triply periodic minimal surface (TPMS) structures have attracted considerable attention due to their mathematically defined, continuous, and interconnected geometries.

Among the various triply periodic minimal surface (TPMS) topologies, the Gyroid structure is widely recognized as one of the most mechanically efficient lattice architectures. Its smooth and continuous geometry promotes uniform stress distribution and effective load transfer, resulting in superior compressive performance compared with conventional grid-based structures (Guo et al., 2023). The interconnected pore network also provides a high surface-to-volume ratio, excellent specific energy absorption, and an exceptional strength-to-density ratio, making Gyroid lattices attractive for lightweight structural applications (Bedoya et al., 2025; Justino Netto et al., 2024). Furthermore, the mechanical response of Gyroid structures is strongly influenced by their geometric configuration, with axially aligned designs exhibiting higher stiffness, compressive strength, and energy absorption capacity, reflecting their orientation-dependent anisotropic behaviour (El-Asfoury et al., 2026). Beyond mechanical applications, their highly interconnected channels facilitate fluid transport and provide favourable conditions for cell attachment, proliferation, and migration, which has driven increasing interest in biomedical applications (Junaedi et al., 2024). Nevertheless, the performance of Gyroid lattices is governed not only by topology but also by factors such as relative density, unit-cell size, wall thickness, printing resolution, and process-induced defects. Experimental studies on FDM-printed polymer TPMS lattices have shown that these parameters significantly affect stiffness, compressive strength, energy absorption, deformation behaviour, and failure mechanisms, highlighting the importance of optimizing both architectural design and manufacturing conditions to achieve superior structural performance (Razi et al., 2024; Saleh et al., 2022).

Despite the growing interest in Gyroid-based structures for lightweight engineering and biomedical applications, important gaps remain in the understanding of their mechanical performance. Previous studies on TPMS lattices have focused primarily on compressive behaviour and topology comparisons, while tensile and flexural responses have received considerably less attention (El-Asfoury et al., 2026; Kladovasilakis et al., 2021). As a result, the combined effects of relative density (infill density) and layer thickness on the tensile and flexural properties of FDM-printed polylactic acid (PLA) Gyroid structures, as well as their associated fracture mechanisms, remain poorly understood. This knowledge gap is particularly significant because tensile and flexural loading are more sensitive to manufacturing-induced imperfections, such as interlayer defects, incomplete fusion, voids, and geometric inaccuracies, which can accelerate crack initiation and propagation and ultimately influence failure behaviour. Therefore, a systematic investigation of the combined influence of relative density and layer thickness on the tensile, flexural, and fracture behaviour of FDM-printed PLA Gyroid structures is required to establish clearer structure-property relationships and support the optimization of high-performance lightweight components.

To address these limitations, the present work investigates the mechanical behaviour and failure characteristics of FDM-printed PLA Gyroid porous structures under tensile and flexural loading conditions. The combined effects of infill density (30%, 50%, and 70%) and layer thickness (0.3, 0.4, and 0.5 mm) were evaluated to determine their influence on mechanical performance. Furthermore, the behaviour of Gyroid specimens was compared with that of nominally solid PLA specimens used as control samples, enabling the mechanical trade-offs associated with the introduction of a porous architecture to be quantified. Field Emission Scanning Electron Microscopy (FESEM) was also employed to examine fracture surfaces and failure characteristics, providing further insight into the relationships among processing parameters, structural features, and mechanical properties.

MATERIALS AND EXPERIMENTAL METHODOLOGY

Material Specifications

Commercial-grade PLA Pro filament (grey appearance) with a nominal diameter of 1.75 mm was utilized as the primary feedstock material. Prior to specimen fabrication, the raw filament was inspected using a Leica DVM6 digital microscope to verify dimensional uniformity and confirm the absence of surface defects that could cause unstable extrusion. No evidence of surface micro-cracks, inclusions, or moisture-induced swelling.

Design and Slicing Configurations

The computer-aided design (CAD) models for the mechanical characterization specimens were developed using CAD software in accordance with the relevant ASTM standards. Tensile test specimens were designed based on the ASTM D638 Type I standard geometry, adopting a dog-bone configuration with overall dimensions of 165 mm × 19 mm × 3.2 mm and a gauge length of 57 mm. For flexural testing, rectangular bar specimens were modeled following the ASTM D790 standard, with dimensions of 127 mm × 12.7 mm × 3.2

mm. The use of standardized specimen geometries ensured consistency in sample preparation and enabled reliable comparison of the mechanical properties obtained during tensile and flexural evaluations.

The generated CAD models were imported into CreatWare slicing software for toolpath generation and print preparation. A continuous gyroid infill architecture was applied to all porous specimens to maintain a consistent internal topology throughout the experimental programme. Two processing parameters were systematically varied: infill density and layer thickness. Infill density was investigated at three levels (30%, 50%, and 70%), corresponding to nominal porosities of 70%, 50%, and 30%, respectively, while layer thickness was varied at 0.3, 0.4, and 0.5 mm. These parameter combinations were selected to specifically evaluate the individual and interactive effects of infill density and layer thickness on the tensile and flexural performance of the gyroid structures. Other printing and architectural parameters were maintained constant wherever applicable to minimize confounding effects. Fully dense specimens (100% infill) fabricated at the same layer thicknesses were included as reference controls. Table 1 summarizes the experimental design configurations.

Table 1: Experimental design matrix and printing parameter configurations

Specimen Designation (Sample ID)	**Infill Density (%)**	**Infill Pattern**	**Layer Thickness (mm)**
S1	30	Gyroid	0.3
S2	30	Gyroid	0.4
S3	30	Gyroid	0.5
S4	50	Gyroid	0.3
S5	50	Gyroid	0.4
S6	50	Gyroid	0.5
S7	70	Gyroid	0.3
S8	70	Gyroid	0.4
S9	70	Gyroid	0.5
S10 (Control specimen)	100	Solid	0.3
S11 (Control specimen)	100	Solid	0.4
S12 (Control specimen)	100	Solid	0.5

The gyroid topology was maintained for all porous specimens. Other documented FDM processing parameters were held constant at a nozzle diameter of 0.8 mm, nozzle temperature of 210°C, bed temperature of 60°C, and printing speed of 50 mm/s.

Fabrication Setup

Fabrication was performed using an industrial-grade CreatBot D1000 FDM 3D printer equipped with a fully enclosed thermal chamber. To isolate the effects of the two investigated variables, namely infill density and layer thickness, the remaining documented machine-processing parameters were maintained constant throughout specimen fabrication. A nozzle diameter of 0.8 mm, nozzle temperature of 210°C, bed temperature of 60°C, and printing speed of 50 mm/s were used for all specimens. Maintaining these parameters at fixed values reduced potential variability associated with thermal and deposition conditions, allowing the observed differences in mechanical performance to be primarily evaluated in relation to the systematically varied infill density and layer thickness.

Mechanical Characterization

All mechanical characterizations were performed using a SHIMADZU Universal Testing Machine (UTM) equipped with a 100 kN load cell. Three replicate specimens were tested for each investigated printing condition to assess the repeatability of the mechanical response. Tensile testing was conducted in accordance with ASTM D638 at a constant crosshead speed of 5 mm/min. During testing, the applied load and corresponding elongation were recorded continuously and subsequently used to determine the engineering stress and strain values. The uniaxial stress (σ) and strain (ε) were calculated using Equations (1) and (2), respectively.

$$\sigma = \frac{F}{A} \quad (1)$$

$$\epsilon = \frac{\Delta L}{L} \quad (2)$$

where F is the recorded force, A is the initial cross-sectional area, ΔL is the crosshead displacement, and L is the original gauge length.

Flexural testing was carried out in accordance with the ASTM D790 standard using a three-point bending fixture mounted on a SHIMADZU Universal Testing Machine (UTM). The tests were performed at a constant crosshead speed of 2 mm/min using a three-point bending configuration, over a fixed support span to assess the bending behaviour of the fabricated specimens. During testing, the applied load and corresponding mid-span deflection were continuously recorded Flexural stress (σ_f) and flexural strain (ϵ_f) were derived using Equations (3) and (4):

$$\sigma_f = \frac{3FL_s}{2bd^2} \quad (3)$$

$$\epsilon_f = \frac{6Dd}{L_s^2} \quad (4)$$

For each printing condition, three replicate specimens (n = 3) were mechanically tested. The mechanical properties are reported as the mean of the three measurements to account for specimen-to-specimen variability and assess experimental repeatability. Experimental variability was quantified using the standard deviation of the three replicate measurements for each printing condition. A formal measurement-uncertainty budget was not established because calibration uncertainty and instrument-specific uncertainty components were not available for the present dataset. Therefore, the reported standard deviations represent the observed experimental variability rather than the expanded measurement uncertainty of the testing system. A two-way analysis of variance (ANOVA) was performed to evaluate the effects of infill density and layer thickness, including their interaction, on tensile and flexural strength. Statistical significance was assessed at a 95% confidence level, with $p < 0.05$ considered statistically significant.

Morphological and Microstructural Analysis

Following mechanical testing, selected fracture surfaces were coated with a thin conductive gold layer and imaged using Field Emission Scanning Electron Microscopy (FESEM). FESEM micrographs were analyzed to evaluate internal pore geometry, filament packing density, interlayer adhesion quality, and microstructural failure modes.

RESULTS AND DISCUSSION

To statistically evaluate the effects of the investigated printing parameters on mechanical performance, a two-way ANOVA was performed for tensile and flexural strength, considering infill density and layer thickness as the main factors. The corresponding ANOVA results are presented in Table 2.

Table 2: Two-way ANOVA results for the effects of infill density and layer thickness on tensile and flexural strength

Response	Source	F-value	p-value	Statistical significance
Tensile strength	Infill density	152.76	<0.001	Significant
	Layer thickness	152.83	<0.001	Significant
	Infill density × Layer thickness	5.10	0.006	Significant
Flexural strength	Infill density	48.96	<0.001	Significant
	Layer thickness	72.72	<0.001	Significant
	Infill density × Layer thickness	6.78	0.002	Significant

Statistical significance was evaluated at a 95% confidence level ($p < 0.05$). The analysis was performed using the porous gyroid specimens (30%, 50%, and 70% infill density), with three replicate specimens ($n = 3$) for each parameter combination. Fully solid specimens were treated as reference controls and were not included in the factorial ANOVA.

As shown in Table 2, both infill density and layer thickness had statistically significant effects on tensile strength ($p < 0.001$). The comparable F-values obtained for infill density ($F = 152.76$) and layer thickness ($F = 152.83$) indicate that both parameters strongly contributed to the variation in tensile strength within the investigated parameter range. A statistically significant interaction between infill density and layer thickness was also observed ($F = 5.10$, $p = 0.006$), indicating that the effect of layer thickness on tensile strength depended on the selected infill density. For flexural strength, both infill density ($F = 48.96$, $p < 0.001$) and layer thickness ($F = 72.72$, $p < 0.001$) were statistically significant, with the larger F-value for layer thickness suggesting a stronger contribution to the flexural response within the investigated conditions. The interaction between infill density and layer thickness was also significant ($F = 6.78$, $p = 0.002$), demonstrating that these parameters did not act independently in determining the mechanical response of the porous PLA structures.

Tensile Mechanical Performance

Tensile testing was performed to evaluate the mechanical response of FDM-fabricated porous PLA structures with varying infill densities and layer thicknesses. The measured tensile properties are presented in Table 3. Overall, both infill density and layer thickness influenced the tensile performance of the printed specimens.

Prior to comparing the effects of the printing parameters, the repeatability of the tensile response was assessed using three replicate specimens for each investigated condition. The replicate stress–strain curves exhibited similar profiles, with closely comparable elastic responses, maximum stresses, and fracture behaviour. Only minor variations in peak stress and strain at failure were observed, which were attributed to inherent variations in filament deposition and interlayer bonding during FDM fabrication. Overall, the agreement among the replicate specimens indicated satisfactory experimental repeatability across the investigated printing conditions.

Table 3: Tensile properties of FDM-printed porous and solid PLA samples

Specimen Designation (Sample ID)	Infill Density (%)	Infill Pattern	Layer Thickness (mm)	Tensile strength (MPa), Mean
S1	30	Gyroid	0.3	25.48 ± 0.21

ISSN No. 2454-6186 | DOI: 10.47772/IJRISS | Volume X Issue VII July 2026

S2	30	Gyroid	0.4	23.74 ± 0.67
S3	30	Gyroid	0.5	28.89 ± 0.18
S4	50	Gyroid	0.3	26.91 ± 0.62
S5	50	Gyroid	0.4	23.46 ± 0.75
S6	50	Gyroid	0.5	28.10 ± 0.64
S7	70	Gyroid	0.3	31.61 ± 0.22
S8	70	Gyroid	0.4	27.32 ± 0.84
S9	70	Gyroid	0.5	32.38 ± 0.84
S10 (Control specimen)	100	Solid	0.3	42.92 ± 0.51
S11 (Control specimen)	100	Solid	0.4	44.26 ± 0.26
S12 (Control specimen)	100	Solid	0.5	46.50 ± 0.65

Note for Table 3: The mean values are based on three replicate specimens ($n = 3$) for each printing condition.

The mean tensile strength of the porous PLA specimens ranged from 23.46 ± 0.75 MPa to 32.38 ± 0.84 MPa, depending on the infill density and layer thickness. In comparison, the fully solid specimens exhibited higher mean tensile strengths ranging from 42.92 ± 0.51 MPa to 46.50 ± 0.65 MPa. The relatively small standard deviations observed for most conditions indicate good repeatability of the tensile measurements and consistency of the FDM fabrication process. As expected, the solid specimens exhibited superior load bearing capability due to the absence of internal voids and the presence of a continuous load-transfer network throughout the material (Yang, 2025). Stress-strain behaviour of all specimens exhibited a predominantly linear elastic region followed by abrupt fracture, indicating the relatively brittle nature of PLA under tensile loading (Ramos et al., 2025). Limited plastic deformation was observed prior to failure, which is characteristic of FDM-printed PLA components where crack initiation and propagation are strongly influenced by inter-layer bonding and internal structural discontinuities (Zhang et al., 2019). The results demonstrate that optimization of printing parameters can substantially improve the mechanical efficiency of porous structures while maintaining significant material savings.

Two-way ANOVA showed that both infill density and layer thickness had statistically significant effects on tensile strength. Infill density produced a significant main effect ($F = 152.76$, $p < 0.001$), while layer thickness also significantly affected tensile strength ($F = 152.83$, $p < 0.001$). In addition, a significant interaction between infill density and layer thickness was observed ($F = 5.10$, $p = 0.006$), indicating that the influence of layer thickness on tensile strength depended partly on the selected infill density. In addition to these statistical effects, the relatively small standard deviations observed for most tensile-strength measurements indicate good repeatability among the replicate specimens. However, the reported mean values represent experimental variability rather than formal measurement uncertainty.

Effect of Infill Density on Tensile Behavior

The stress-strain curves of all porous and solid PLA specimens exhibited predominantly linear elastic behaviour followed by abrupt brittle fracture, as evidenced by the rapid load drop after reaching the ultimate tensile strength. This failure mode is characteristic of FDM-printed PLA due to its limited ductility and relatively weak interlayer bonding (Zhang et al., 2019).

Tensile performance increased with increasing infill density. At a constant layer thickness of 0.5 mm, increasing the infill density from 30% to 70% increased the mean tensile strength from 28.89 ± 0.18 MPa to 32.38 ± 0.84 MPa, corresponding to an improvement of approximately 12.1%. The fully solid specimen exhibited a substantially higher mean tensile strength of 46.50 ± 0.65 MPa. Consistent with these experimental trends, the two-way ANOVA confirmed that infill density significantly affected tensile strength ($p < 0.001$), while its interaction with layer thickness was also statistically significant ($p = 0.006$). The improvement in tensile strength with increasing infill density is primarily attributed to the reduction in internal voids and the greater effective load-bearing area, which facilitate more efficient stress transfer throughout the printed structure (Aboelella et al., 2025; Zhang et al., 2019).

The gyroid infill architecture further contributed to the enhanced tensile behaviour by providing continuous and interconnected load paths, resulting in more uniform stress distribution and reduced stress concentration (Abueidda et al., 2019). In contrast, specimens with lower infill densities contained larger pore regions that acted as stress concentration sites, promoting premature crack initiation and propagation under tensile loading. Consequently, the 30% infill specimens exhibited lower strength and load-carrying capacity despite offering material and printing-time savings.

Interestingly, the elastic modulus did not exhibit a consistent increasing trend with increasing infill density. For example, the 30% infill specimens printed at a 0.5 mm layer thickness exhibited a mean elastic modulus of 1.05 ± 0.15 GPa. This suggests that stiffness is influenced not only by infill density but also by factors such as interlayer adhesion, filament deposition quality, and geometric variability within the printed structure.

Effect of Layer Thickness on Tensile Behavior

Layer thickness also influenced the tensile properties of the printed specimens. For the investigated infill densities, specimens fabricated with a 0.5 mm layer thickness generally exhibited higher tensile strength than those printed with 0.3 mm or 0.4 mm layers. At 70% infill density, the mean tensile strength increased from 31.61 ± 0.22 MPa at 0.3 mm to 32.38 ± 0.84 MPa at 0.5 mm, while the mean maximum force increased from 1313.77 ± 11.43 N to 1347.17 ± 34.85 N.

Under the processing conditions employed in this study, the improved performance observed at the larger layer thickness can be attributed to enhanced filament bonding and reduced interfacial defects (Allum et al., 2023). The use of a 0.8 mm nozzle combined with a 0.5 mm layer height results in wider extrusion tracks and larger contact areas between adjacent rasters. These conditions facilitate stronger inter-bead fusion and improve stress transfer across filament interfaces during tensile loading (Allum et al., 2023). Furthermore, thicker layers reduce the total number of deposited layers required to fabricate a specimen, thereby minimizing the number of inter-layer boundaries that may act as potential crack initiation sites (Syrlybayev et al., 2021). Conversely, specimens printed using thinner layers contain a larger number of interfaces throughout the structure. Although thinner layers generally improve dimensional accuracy and surface finish, the increased number of inter-layer boundaries may introduce additional weak regions where crack propagation can occur. This phenomenon likely contributed to the lower tensile strengths observed for the 0.3 mm and 0.4 mm specimens.

The failure strain data also indicate that layer thickness affected the deformation behaviour of the printed specimens, although the trend was less consistent than that observed for tensile strength. Variations in strain at failure may be associated with differences in interfacial bonding, local pore distribution, and filament deposition quality, which influence the ability of the printed structure to redistribute tensile stresses prior to fracture.

Mechanical Efficiency of Porous Gyroid Structures Based on the Tensile Mechanical Performance

An important observation from this study is the relatively high mechanical efficiency achieved by the porous gyroid structures. The 70% gyroid specimen fabricated with a 0.5 mm layer thickness achieved a mean tensile strength of 32.38 ± 0.84 MPa, corresponding to approximately 69.6% of the mean tensile strength of the fully solid specimen (46.50 ± 0.65 MPa), while reducing the nominal material usage by approximately 30%.

ISSN No. 2454-6186 | DOI: 10.47772/IJRISS | Volume X Issue VII July 2026

This result highlights the effectiveness of the gyroid topology in balancing mechanical performance and material efficiency. The continuous triply periodic minimal surface structure provides favourable load-transfer characteristics while maintaining a lightweight architecture. Such characteristics are particularly beneficial for applications where weight reduction, reduced material usage, and shorter manufacturing times are desirable without excessively sacrificing structural performance.

Overall, both infill density and layer thickness exerted strong effects on tensile strength, with a statistically significant interaction between the two parameters ($p = 0.006$). This interaction indicates that the effect of layer thickness on tensile strength depended on the infill-density condition. Among the investigated porous configurations, the combination of 70% gyroid infill density and 0.5 mm layer thickness produced the highest mean tensile strength (32.38 ± 0.84 MPa), representing a favourable balance between strength retention and nominal material savings. This configuration therefore shows potential for lightweight engineering applications fabricated through fused deposition modelling.

Flexural Mechanical Performance

The flexural properties of the porous PLA specimens are summarized in Table 4. For each printing condition, three replicate specimens were tested, and the maximum force, flexural strength, flexural modulus, and strain are reported as mean ± standard deviation. The results demonstrate variations in flexural response with both infill density and layer thickness.

Table 4: Experimental Flexural Test Results for Porous PLA Specimens

Infill	**Layer**	**Maximum Force (N)**	**Flexural Strength (MPa)**	**Flexural Modulus (GPa)**	**Strain (%)**
30%	0.3	85.76 ± 4.69	49.45 ± 2.70	1.44 ± 0.07	3.45 ± 0.36
30%	0.4	90.77 ± 8.43	52.35 ± 4.86	1.53 ± 0.04	3.41 ± 0.22
30%	0.5	106.94 ± 1.56	61.67 ± 0.90	1.79 ± 0.01	3.45 ± 0.08
50%	0.3	84.69 ± 2.65	48.84 ± 1.53	1.51 ± 0.03	3.22 ± 0.02
50%	0.4	72.55 ± 3.73	41.85 ± 2.15	1.47 ± 0.08	2.85 ± 0.16
50%	0.5	102.76 ± 1.68	59.26 ± 0.98	1.86 ± 0.06	3.18 ± 0.06
70%	0.3	96.92 ± 2.17	55.90 ± 1.26	1.47 ± 0.09	3.81 ± 0.29
70%	0.4	102.86 ± 2.65	59.32 ± 1.53	1.76 ± 0.08	3.38 ± 0.16
70%	0.5	114.25 ± 1.96	65.89 ± 1.13	1.91 ± 0.07	3.45 ± 0.16
Solid	0.3	109.95 ± 0.63	63.41 ± 0.36	1.61 ± 0.09	3.94 ± 0.24
Solid	0.4	106.54 ± 3.86	61.44 ± 2.23	1.77 ± 0.03	3.48 ± 0.10
Solid	0.5	119.68 ± 2.99	69.02 ± 1.71	2.03 ± 0.14	3.40 ± 0.25

Note for Table 4: The mean values are based on three replicate specimens ($n = 3$) for each printing condition.

Two-way ANOVA indicated that both infill density and layer thickness significantly affected flexural strength. Infill density showed a significant main effect ($F = 48.96$, $p < 0.001$), while layer thickness also had a significant effect ($F = 72.72$, $p < 0.001$). A significant interaction between infill density and layer thickness was also identified ($F = 6.78$, $p = 0.002$), demonstrating that the effect of layer thickness on flexural strength varied depending on the infill-density condition.

Effect of Infill Density on Flexural Behaviour

Flexural performance was strongly influenced by infill density. The highest mean flexural strength among the porous specimens (65.89 ± 1.13 MPa) was achieved by the 70% gyroid specimens printed at a 0.5 mm layer thickness. The two-way ANOVA confirmed that infill density significantly affected flexural strength ($p < 0.001$), with a significant interaction between infill density and layer thickness ($p = 0.002$). Increasing the infill density reduced the internal void fraction and increased the effective load-bearing area, enabling the structure to resist bending stresses more effectively. Furthermore, the continuous gyroid geometry promoted more uniform stress distribution and reduced stress concentration, resulting in improved flexural strength and stiffness.

Effect of Layer Thickness on Mechanical Behaviour

Layer thickness influenced both tensile and flexural performance. Across the investigated infill densities, specimens fabricated with a 0.5 mm layer thickness generally exhibited higher mechanical properties. For solid specimens, the mean tensile strength increased from 42.92 ± 0.51 MPa to 46.50 ± 0.65 MPa as the layer thickness increased from 0.3 mm to 0.5 mm, while the 70% gyroid specimens exhibited a smaller increase from 31.61 ± 0.22 MPa to 32.38 ± 0.84 MPa. Similarly, the mean flexural strength of the 70% gyroid specimens increased from 55.90 ± 1.26 MPa to 65.89 ± 1.13 MPa, accompanied by an increase in the mean flexural modulus from 1.47 ± 0.09 GPa to 1.91 ± 0.07 GPa. Within the investigated processing parameters, the improved performance at the 0.5 mm layer thickness may be attributed to enhanced interlayer bonding associated with thicker deposited rasters and fewer interfacial boundaries. A reduction in mechanical performance observed at the intermediate layer thickness of 0.4 mm may be associated with suboptimal bead overlap and localized micro-void formation compared with the 0.5 mm condition.

Structural Efficiency of Gyroid Structures

The 70% gyroid specimen printed at a 0.5 mm layer thickness demonstrated the most favourable balance between mechanical performance and material usage among the porous configurations investigated. This configuration achieved a mean tensile strength of 32.38 ± 0.84 MPa, corresponding to approximately 69.6% of the mean tensile strength of the fully solid specimen (46.50 ± 0.65 MPa), while reducing the nominal material usage by approximately 30%. These findings indicate that the 70% gyroid configuration can provide substantial material savings while retaining approximately 70% of the tensile strength of the fully solid structure, highlighting its potential for lightweight structural applications.

Comparative Analysis: Porous vs. Solid Structures

Comparing the porous structures with the fully solid specimens highlights the trade-off between mechanical performance and material efficiency. As expected, the fully solid specimen printed at a 0.5 mm layer thickness exhibited a substantially higher mean tensile strength of 46.50 ± 0.65 MPa due to its continuous material network and absence of designed internal voids. In contrast, the best-performing porous configuration, consisting of 70% gyroid infill printed at the same layer thickness, achieved a mean tensile strength of 32.38 ± 0.84 MPa, retaining approximately 69.6% of the mean tensile strength of the solid counterpart while providing a nominal material reduction of approximately 30%. This strength retention relative to the reduction in nominal material usage demonstrates the potential of the gyroid TPMS architecture for maintaining structural performance in porous components. The continuous and interconnected geometry promotes efficient load transfer and stress redistribution, allowing the porous structure to sustain mechanical loads despite the presence of designed internal voids (Abueidda et al., 2019). From an engineering perspective, the porous gyroid structures therefore offer a favourable trade-off between material reduction and mechanical performance. While fully solid structures remain preferable for applications requiring maximum load-bearing capacity, the 70% gyroid configuration provides substantial nominal material savings while retaining approximately 70% of the tensile strength of the corresponding solid structure. This characteristic makes gyroid-based porous structures promising for lightweight components where material efficiency and reduced manufacturing resource consumption are important design considerations.

The observed mechanical trends should be interpreted within the specific processing and architectural conditions investigated in this study. Infill density and layer thickness were systematically varied, whereas the documented machine-processing parameters, including nozzle diameter (0.8 mm), nozzle temperature (210 °C), bed temperature (60 °C), and printing speed (50 mm/s), were maintained constant, to isolate the effects of the investigated variables. Other parameters that may influence the mechanical response of FDM-fabricated gyroid structures, such as build orientation and additional architectural characteristics, were not systematically varied. Consequently, the mechanical trends and statistically significant effects identified in this study are specific to the parameter range investigated and should not be generalized to all FDM processing conditions or gyroid configurations.

Although the interconnected porosity of gyroid structures may offer potential for biomedical scaffold applications, the present study evaluated only their mechanical and microstructural behaviour. Biological performance, including biocompatibility and cellular response, was not investigated. Therefore, the present findings should be interpreted as evidence of mechanical potential rather than confirmation of biomedical suitability

Microstructural Fracture Morphology

High Infill Density (70% Gyroid) Morphology

Figure 1 presents the fracture morphology of the specimen fabricated with a 70% infill density. FESEM observations revealed a highly compact filament arrangement with dense packing of adjacent gyroid walls and only small, isolated interstitial voids distributed throughout the cross-section. The large contact area between neighboring rasters promoted effective thermal diffusion and strong neck formation during deposition, resulting in enhanced interlayer bonding. The fracture surface exhibited non-planar and tortuous crack propagation paths that traversed both filament bodies and interface boundaries rather than propagating exclusively along layer interfaces. Such crack behavior indicates a high resistance to crack growth and reflects efficient stress redistribution throughout the cellular structure. Furthermore, the fracture morphology revealed evidence of cohesive matrix failure accompanied by localized inter-bead shear, suggesting that the strength of the interlayer bonds approached that of the bulk material. These observations confirm that the continuous gyroid architecture facilitated effective load transfer across the component volume, thereby contributing to the superior mechanical performance observed at higher infill densities (Abueidda et al., 2019).

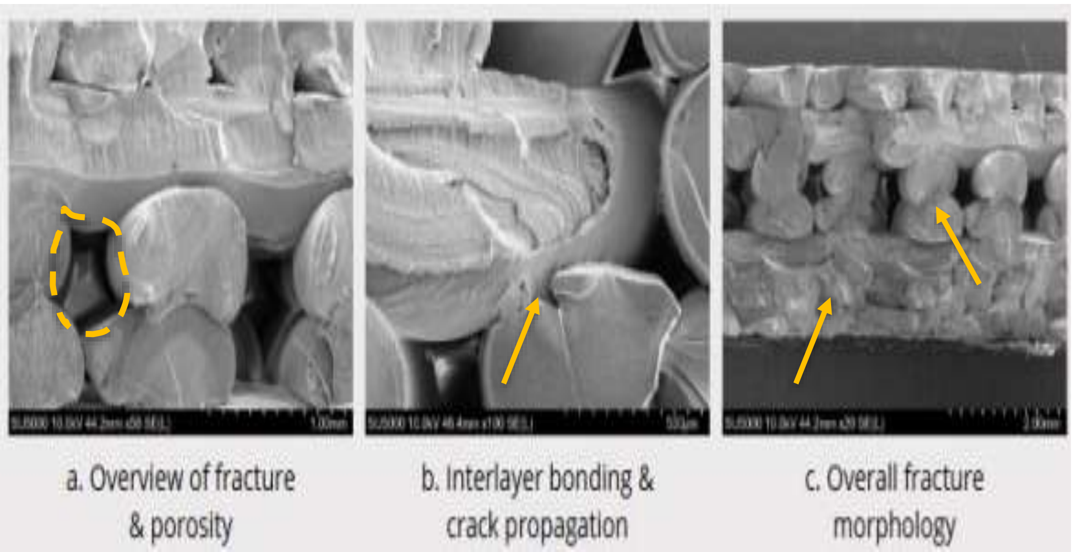

Figure 1: Representative FESEM fracture surface micrographs of FDM-printed porous PLA with 70% infill density

Low Infill Density (30% Gyroid)

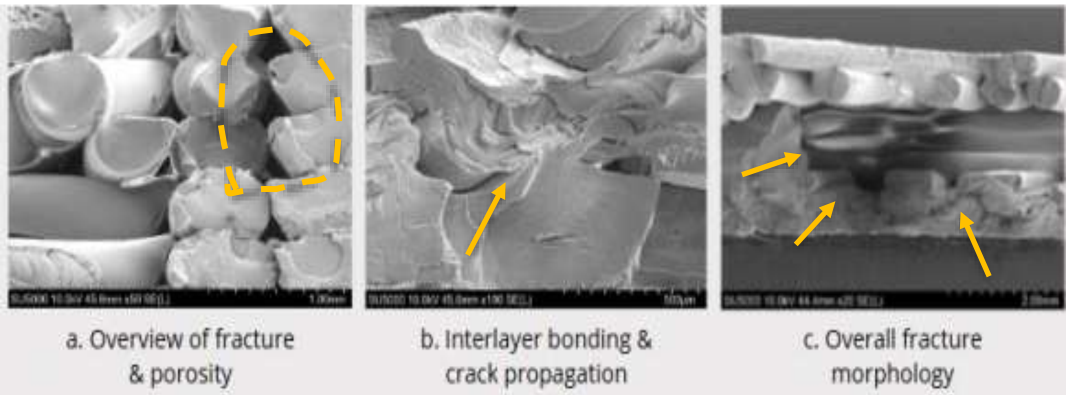

Figure 2. Representative FESEM fracture surface micrographs of FDM-printed porous PLA with 30% infill density.

Figure 2 presents the fracture morphology of the specimen fabricated with a 30% infill density. FESEM observations revealed a porous internal structure characterized by large, interconnected inter-filament voids and relatively thin gyroid walls. The reduced contact area between adjacent deposited rasters limited thermal diffusion and neck formation during printing, resulting in weaker interfacial bonding and the presence of localized stress concentration regions within the structure. Under tensile loading, crack initiation occurred preferentially at these weakly bonded interfaces, leading to premature failure through extensive interlayer delamination and filament pull-out (Banić et al., 2024; Zhang et al., 2019). The fracture surface was predominantly smooth and exhibited minimal plastic deformation, indicating that failure was governed primarily by interfacial debonding rather than cohesive matrix yielding. Furthermore, the large open void channels acted as macro-scale stress concentrators that facilitated rapid crack propagation across the structure. These observations suggest that the lower infill density reduced the effectiveness of load transfer between adjacent filaments, thereby contributing to the lower tensile strength and reduced mechanical stability observed in the 30% infill specimens.

CONCLUSIONS

This study investigated the effects of gyroid infill density and layer thickness on the tensile, flexural, and microstructural behaviour of FDM-fabricated porous PLA structures. Both parameters significantly influenced tensile and flexural strength ($p < 0.001$), with significant interactions between infill density and layer thickness. Among the porous configurations, the 70% gyroid infill fabricated at a 0.5 mm layer thickness provided the most favourable mechanical performance, achieving a mean tensile strength of 32.38 ± 0.84 MPa and flexural strength of 65.89 ± 1.13 MPa. The tensile strength corresponded to approximately 69.6% of that of the fully solid specimen (46.50 ± 0.65 MPa), while providing a nominal material reduction of approximately 30%. FESEM observations supported the mechanical results, with lower-density specimens exhibiting larger voids, interlayer delamination, and filament pull-out, whereas higher-density structures showed more cohesive fracture and improved load-transfer characteristics. Overall, the findings demonstrate that gyroid architecture can provide a favourable balance between mechanical performance and material efficiency, particularly for lightweight engineering applications. The conclusions are limited to the investigated infill densities (30–70%) and layer thicknesses (0.3–0.5 mm) under the fixed printing conditions used in this study. Future work should examine additional FDM and architectural parameters, including build orientation, printing temperature and speed, and unit-cell geometry, together with compression, fatigue, and impact behaviour. Biological evaluation is also required before extending the present mechanical findings to biomedical scaffold applications.

ACKNOWLEDGEMENTS

The authors gratefully acknowledge the financial support provided by Universiti Teknikal Malaysia Melaka (UTeM) through the PJP University Research Grant year 2025 (Grant No. PJP/2025/FTKIP/PERSPEKTIF/SA0098). The authors also sincerely appreciate the research facilities, technical support, and resources provided by UTeM, which contributed significantly to the successful completion of this study.

REFERENCES

1. Aboelella, M. G., Ebeid, S. J., & Sayed, M. M. (2025). Layer combination of similar infill patterns on the tensile and compression behavior of 3D printed PLA. Scientific Reports, 15(1). https://doi.org/10.1038/s41598-025-94446-8
2. Abueidda, D. W., Elhebeary, M., Shiang, C. S. (Andrew), Pang, S., Abu Al-Rub, R. K., & Jasiuk, I. M. (2019). Mechanical properties of 3D printed polymeric Gyroid cellular structures: Experimental and finite element study. Materials and Design, 165. https://doi.org/10.1016/j.matdes.2019.107597
3. Allum, J., Moetazedian, A., Gleadall, A., Mitchell, N., Marinopoulos, T., McAdam, I., Li, S., & Silberschmidt, V. V. (2023). Extra-wide deposition in extrusion additive manufacturing: A new convention for improved interlayer mechanical performance. Additive Manufacturing, 61. https://doi.org/10.1016/j.addma.2022.103334
4. Banić, D., Itrić Ivanda, K., Vukoje, M., & Cigula, T. (2024). Impact Fracture Resistance of Fused Deposition Models from Polylactic Acid with Respect to Infill Density and Sample Thickness. Applied Sciences (Switzerland), 14(5). https://doi.org/10.3390/app14052035
5. Bedoya, M. C., Restrepo, J. W., Wilches, L. V., & Rodriguez, J. (2025). Cellular Structures Analysis Under Compression Test. Polymers, 17(11). https://doi.org/10.3390/polym17111476
6. Calabrese, L., Marabello, G., Chairi, M., & Di Bella, G. (2025). Optimization of Deposition Temperature and Gyroid Infill to Improve Flexural Performance of PLA and PLA–Flax Fiber Composite Sandwich Structures. Journal of Manufacturing and Materials Processing, 9(2). https://doi.org/10.3390/jmmp9020031
7. Cojocaru, V., Frunzaverde, D., Miclosina, C. O., & Marginean, G. (2022). The Influence of the Process Parameters on the Mechanical Properties of PLA Specimens Produced by Fused Filament Fabrication—A Review. In Polymers (Vol. 14, Number 5). MDPI. https://doi.org/10.3390/polym14050886
8. de Mulder, E. L. W., Buma, P., & Hannink, G. (2009). Anisotropic porous biodegradable scaffolds for musculoskeletal tissue engineering. Materials, 2(4), 1674–1696. https://doi.org/10.3390/ma2041674
9. Ekşi, S., & Karakaya, C. (2025). Effects of Process Parameters on Tensile Properties of 3D-Printed PLA Parts Fabricated with the FDM Method. Polymers, 17(14). https://doi.org/10.3390/polym17141934
10. El-Asfoury, M. S., El-Bedwehy, N. E., Shazly, M., & Elkaseer, A. (2026). Orientation driven design and mechanical optimization of gyroid TPMS lattice structures. Scientific Reports, 16(1). https://doi.org/10.1038/s41598-026-35201-5
11. Guo, W., Yang, Y., Liu, C., Bu, W., Guo, F., Li, J., Wang, E., Peng, Z., Mai, H., You, H., & Long, Y. (2023). 3D printed TPMS structural PLA/GO scaffold: Process parameter optimization, porous structure, mechanical and biological properties. Journal of the Mechanical Behavior of Biomedical Materials, 142. https://doi.org/10.1016/j.jmbbm.2023.105848
12. Junaedi, H., Abd El-baky, M. A., Awd Allah, M. M., & Sebaey, T. A. (2024). Mechanical Characteristics of Sandwich Structures with 3D-Printed Bio-Inspired Gyroid Structure Core and Carbon Fiber-Reinforced Polymer Laminate Face-Sheet. Polymers, 16(12). https://doi.org/10.3390/polym16121698
13. Justino Netto, J., Sardinha, M., & Leite, M. (2024). Influence of the cell size and wall thickness on the compressive behaviour of fused filament fabricated PLA gyroid structures. Mechanics of Materials, 195. https://doi.org/10.1016/j.mechmat.2024.105051
14. Kladovasilakis, N., Tsongas, K., & Tzetzis, D. (2021). Mechanical and fea-assisted characterization of fused filament fabricated triply periodic minimal surface structures. Journal of Composites Science, 5(2). https://doi.org/10.3390/jcs5020058
15. Marșavina, L., Vălean, C., Mărghitaș, M., Linul, E., Razavi, N., Berto, F., & Brighenti, R. (2022). Effect of the manufacturing parameters on the tensile and fracture properties of FDM 3D-printed PLA specimens. Engineering Fracture Mechanics, 274. https://doi.org/10.1016/j.engfracmech.2022.108766

16. Megersa, G. K., Sitek, W., Nowak, A. J., & Tomašić, N. (2024). Investigation of the Influence of Fused Deposition Modeling 3D Printing Process Parameters on Tensile Properties of Polylactic Acid Parts Using the Taguchi Method. Materials, 17(23). https://doi.org/10.3390/ma17235951
17. Ötüken, R., Alparslan, C., Erhan, M. F., & Bayraktar, Ş. (2026). Reinforcement of Novel PLA/17-4 PH Stainless Steel Hybrid Structures Fabricated by FDM: The Effects of Layer Configuration, Infill Density and Pattern. Polymers, 18(6). https://doi.org/10.3390/polym18060672
18. Pan, Z., & Ding, J. (2012). Poly(lactide-co-glycolide) porous scaffolds for tissue engineering and regenerative medicine. In Interface Focus (Vol. 2, Number 3, pp. 366–377). Royal Society. https://doi.org/10.1098/rsfs.2011.0123
19. Ramos, L. L. B., Iwasaki, K. M. K., Beck, R., Scheffer, W. C., Fuga, F. R., & De Medeiros, R. (2025). Influence of layer orientation on the mechanical properties of fused deposition modelling using PLA and PETG. Materialia, 44. https://doi.org/10.1016/j.mtla.2025.102541
20. Razi, S. S., Pervaiz, S., Susantyoko, R. A., & Alyammahi, M. (2024). Optimization of Environment-Friendly and Sustainable Polylactic Acid (PLA)-Constructed Triply Periodic Minimal Surface (TPMS)-Based Gyroid Structures. Polymers, 16(8). https://doi.org/10.3390/polym16081175
21. Saleh, M., Anwar, S., Al-Ahmari, A. M., & Alfaify, A. (2022). Compression Performance and Failure Analysis of 3D-Printed Carbon Fiber/PLA Composite TPMS Lattice Structures. Polymers, 14(21). https://doi.org/10.3390/polym14214595
22. Syrlybayev, D., Zharylkassyn, B., Seisekulova, A., Akhmetov, M., Perveen, A., & Talamona, D. (2021). Optimisation of strength properties of FDM printed parts—A critical review. In Polymers (Vol. 13, Number 10). MDPI AG. https://doi.org/10.3390/polym13101587
23. Tang, C., Liu, J., Yang, Y., Liu, Y., Jiang, S., & Hao, W. (2020). Effect of process parameters on mechanical properties of 3D printed PLA lattice structures. Composites Part C: Open Access, 3. https://doi.org/10.1016/j.jcomc.2020.100076
24. Yang, B. (2025). The influence of infill density on the mechanical properties of PLA samples in FDM 3D printing. Journal of Physics: Conference Series, 3019(1). https://doi.org/10.1088/1742-6596/3019/1/012046
25. Zhang, X., Chen, L., Mulholland, T., & Osswald, T. A. (2019). Characterization of mechanical properties and fracture mode of PLA and copper/PLA composite part manufactured by fused deposition modeling. SN Applied Sciences, 1(6). https://doi.org/10.1007/s42452-019-0639-5